

Fundamental Framework for Technical Analysis

J. V. Andersen¹, S. Gluzman² and D. Sornette^{1,3}

¹ Nordic Institute for Theoretical Physics

Blegdamsvej 17, DK-2100 Copenhagen, Denmark

² Laboratoire de Physique de la Matière Condensée

CNRS UMR6622 and Université de Nice-Sophia Antipolis

B.P. 71, Parc Valrose, 06108 Nice Cedex 2, France

³ Institute of Geophysics and Planetary Physics

and Department of Earth and Space Science

University of California, Los Angeles, California 90095

Abstract

Starting from the characterization of the past time evolution of market prices in terms of two fundamental indicators, price velocity and price acceleration, we construct a general classification of the possible patterns characterizing the deviation or defects from the random walk market state and its time-translational invariant properties. The classification relies on two dimensionless parameters, the Froude number characterizing the relative strength of the acceleration with respect to the velocity and the time horizon forecast dimensionalized to the training period. Trend-following and contrarian patterns are found to coexist and depend on the dimensionless time horizon. The classification is based on the symmetry requirements of invariance with respect to change of price units and of functional scale-invariance in the space of scenarios. This “renormalized scenario” approach is fundamentally probabilistic in nature and exemplifies the view that multiple competing scenarios have to be taken into account for the same past history. Empirical tests are performed on about nine to thirty years of daily returns of twelve data sets comprising some major indices (Dow Jones, SP500, Nasdaq, DAX, FTSE, Nikkei), some major bonds (JGB, TYX) and some major currencies against the US dollar (GBP, CHF, DEM, JPY). Our “renormalized scenario” exhibits statistically significant predictive power in essentially all market phases. In contrast, a trend following strategy and trend + acceleration following strategy perform well only on different and specific market phases. The value of the “renormalized scenario” approach lies in the fact that it always finds the best of the two, based on a calculation of the stability of their predicted market trajectories.

I. INTRODUCTION

There is increasing evidences that even the most competitive markets are not strictly efficient [9,29]. In particular, a set of studies in the academic finance literature have reported

anomalous earnings which support technical analysis strategies [16,13,18,7] (see [20] for a different view). A recent study of 60 technical indicators on 878 stocks over a 12-year period [5] finds that the trading signals from technical indicators do on average contain information that may be of value in trading, even if they generally underperform (without taking due consideration to risk-adjustments of the returns) a buy-and-hold strategy in a rising market by being relatively rarely invested.

Another class of studies views the market place as a complex self-organizing system [3,9] which suggests that technical analysis may have some value. This approach views the traders develop strategies both fundamental, technical and any mixture of them, which adapt and react to the pattern these strategies create by their collective action. This concept is common to other systems in Nature as well, including ions in a spin glass, cells in an immune system, faults in the crust, etc. In the economy, economic agents, banks, consumers, firms, or investors, continually adjust their market moves, buying decisions, prices, and forecasts to the situation these moves or decisions or prices or forecasts together create. The challenge is to understand how these actions, strategies, and expectations react to and change with the aggregate patterns these create. Since the self-organization is not instantaneous via the processes of adjustment and change as the traders react, the market evolves leading to a novel adjustment of the traders. The market as a complex system is a process that constantly evolve and unfold over time. It might thus exhibit some degree of predictability in contrast to the efficient market hypothesis and the proof that correctly anticipated prices are random [23].

Most trading systems fall into two classes.

- The first one is trend-following: the technical indicators attempt to detect a significant trend and issue a signal for the trader to profit from the trend.
- The second class is contrarian: the technical indicators try to measure a change of trend. For instance, the oscillator indicators, which are used to model the cyclical nature of markets, typically will filter the trend out of prices, leaving only the remaining changes of trends.

Notwithstanding their multiple forms and sometimes complicated formulations [1,22], technical indicators can be seen as reducing essentially to combinations of measurements of

1. a price velocity v , defined as the rate of change of the price (possibly over different time scales), and of
2. a price acceleration g , defined as the rate of change of the price velocity.

The velocity is a measure of the strength of a trend, while the acceleration quantifies its persistence. For instance, when a market has been trending upward and then begins to decelerate, an oscillator indicator will level off, suggesting an approaching market top. Likewise, if a market is trending downward and this trend decelerate, then a bottom would be forecasted by the technical indicators. This phenomenology has suggested qualitative analogies with Newton's law of classical motion, according to which velocities (or momentum) change because market forces are exerting their influence and produce acceleration/deceleration.

This view is in contrast to the (weak) efficient market and random walk hypotheses, deeply ingrained in the financial academic literature, according to which future variations of prices are unpredictable (at least from the sole knowledge of past prices). Here, we develop a fundamental theory of technical analysis based on the idea that trading signals, when they can be identified, quantify local deviations from or equivalently *defects* of the normal random walk state taken as a reference. Expressing the random walk hypothesis as the fully symmetric state of the market, we show that trading patterns corresponds to local breakdowns of this symmetry. Based on simple symmetry principles, we show how to classify the possible patterns based on the measurements of three fundamental dimensionless numbers that are found to characterize a given market regime. The first one is the Froude number defined by

$$F \equiv \frac{v^2}{p_0 g} , \quad (1)$$

where p_0 is the current price level, v (resp. g) is the price velocity (resp. acceleration). It measures the relative strength of the trend with respect to the acceleration/deceleration. The second dimensionless number is the future over past horizon ratio, defined as the ratio of the forecast time over the time interval used for detecting the pattern. The third relevant parameter is the dimensionless time interval T_N used for detecting the pattern, i.e. the reduced dimensionless learning period, expressed as follows,

$$T_N = \frac{v}{p_0} t_N ,$$

where t_N is the learning period, or past horizon, expressed in some dimensional time units (days for instance).

II. FUNDAMENTAL SYMMETRY PRINCIPLES

Consider a time series for the price S of an asset. It is defined as a sequence of $N + 1$ values of the price $S(t_0), S(t_1), \dots, S(t_N)$, given for $N + 1$ equidistant successive moments of time $t = t_j$, where $j = 0, 1, 2 \dots N$. Our aim is to unravel indicators, i.e. departure from randomness, for the level of the price $S(t_N + \Delta t)$ at a later time $t = t_N + \Delta t$, that are compatible with the following five general properties.

- Prices should remain positive, $S > 0$, and their theoretical description should be invariant with respect to a change of units: the number describing the value of a stock changes when expressing it in US dollar or in Euros, but the stock value remains what it is. The detection of a price pattern and a forecast must thus remain invariant with respect to such changes. Within the efficient market hypothesis, this requirement eliminates Bachelier's model of the random walk of prices and replaces it by the random walk of the logarithm of prices [23]. The model of a random walk of the logarithm of the price has, by definition, the symmetry of translational invariance of returns, which in turn is equivalent to the symmetry of scaling invariance of the price: the multiplication of all prices by the same factor does not change their return. Such scale invariance symmetry underlies many natural phenomena and is a strong constraint for theoretical construction [8].

- The theory should be invariant with respect to a change of time unit.
- A sensible theory of prices should not lead to zeros, poles or divergences in finite time, as prices and values are finite.
- Patterns and their associated forecast should be defined in probabilistic terms, allowing for multiple scenarii evolving from the same past evolution; probabilities for different scenarii should be expressed only through historical data, and in the form constrained by the above mentioned demands on the price. Deeply imbedded in our approach is the view of the future as a set of potentially acceptable trajectories that can branch and bifurcate at special times. At certain times, only one main trajectory extrapolates with high probability from the past making the future depend almost deterministically (albeit possibly in a nonlinear and chaotic manner) on the past. At other times, the future is much less certain with multiple almost equivalent choices. In this case, we return to an almost random walk picture. The existence of a unique future must not be taken as the signature of a single dynamical system but as the collapse of the large distribution of probabilities. This is the concept learned for instance from the famous Polya Urn problem in which the historical trajectory appears to converge to a certain outcome, which is however solely controlled by the accumulation of purely random choices; a different outcome might have been selected by history with equal probability [2]. We propose that it is fundamental to view any forecasting program as essentially a quantification of probabilities for possible competing scenerios. This view has been vividly emphasized by Asimov in his famous Science-Fiction “Foundation” series [4].
- We restrict the theoretical formulation to the case where, in absence of the fundamental equations for price dynamics and other knowledge, the future values of the price are constrained only by the past values. In order to reduce substantially the class of possible scenarii, we propose to express this condition in a way that makes apparent a deep symmetry between time evolution and functional mapping. We will explain below how this theoretical program can be formalized by the symmetry of *functional self-similarity* [26].

Our approach can be thought of as a search for a non-autonomous dynamical system, where the law of motion changes with time and its functional form remains unknown. Such a dynamical system is not self-similar in real time, does not have a single dynamical representation, but can be characterized by a functional self-similarity [26]. We do not assume that the basic laws which govern market evolution should remain the same in the future as they were in the past, although they will be obtained from the system’s past. In our approach, they are prescribed to evolve with time, due to the assimilation of new information about the market. One can also think about a window of forecasting detected in the market evolution as a *spontaneous* breaking of continuous translational time invariance (the random walk reference being translationally time invariant in its increments), occurring whenever it is dictated by relative probabilities of the evolution patterns with and without explicit violation of this symmetry.

In addition to these five natural requested properties, we add the concept that

- deviations from the random walk hypothesis are quantified by measurements of the price velocity v and of the price acceleration g .

This additional ingredient is motivated by the following considerations.

1. First, as we recalled in the introduction, most technical trading systems attempt to measure trends and/or change of trends in one way or another. We thus adopt the pragmatic point of view that decades of empirical research by practitioners has unraveled indicators of potential value that may capture useful information.
2. A complementary view point is that the market is self-organized by the action of all traders, many of whom use technical analysis to guide their investment decisions. It thus makes good sense to use indicators that are a decisive part of the creation of the very structure of the market that one tries to detect and from which one would like to forecast. This is in spirit similar to the approach advocated by models of the stock markets viewed as complex self-organized adaptive systems [3].
3. Another argument is that a constant trend in the logarithm of the price simply defines a fixed return rate, which in economic theory can be interpreted as the risk-free interest rate plus the risk premium paid for being invested in the market. The velocity is thus similar to a risk-adjusted return, a fundamental quantity in Portfolio theory and practice. We propose the concept of a “psychological Galilean principle”, according to which investors perceive so-called “market forces” only when trends change. We borrow here on the physiological and psychological evidences [25] that a constant stimulus is progressively endogeneized and decreases progressively from the conscious mind. A variation (acceleration/deceleration) is needed to create a new stimulus. Similarly, we argue that investors are more sensitive, after a while, to change of trends rather than to the continuation of the trend.

III. SCENARIOS AND PROBABILITIES

A. Velocity-acceleration parameterization

The first step of our theoretical construction consists in selecting a parametric representation of the past time series. As we argued above, the information of the past price realizations ending at any given time t_N (called “the present”) is encoded by two parameters, the price velocity $v(t_N)$ and the acceleration $g(t_N)$. The simplest non-trivial use of this parameterization is to form the second-order regression polynomial,

$$S_0(t) = A_0 + A_1 t + A_2 t^2, \quad (2)$$

where $S_0(t)$ is the model price at time $t_0 \leq t \leq t_N$, with coefficients A_0, A_1, A_2 adjusted to the real time series $S(t)$ by a mean-square fit or any other suitable regression technique. The coefficients A_0, A_1, A_2 are obtained as the solutions of a system of a linear algebraic equations derived from the condition of minimal Euclidean distance between the polynomial (2) and historical prices. It is clear that A_1 (resp. A_2) is proportional to the price velocity (resp. acceleration). This representation (2) is reminiscent of

the so-called “parabolic curve pattern” often used in technical analysis (see for instance <http://www.chartpattern.com/paraboliccurve.html>). The parabolic formula follows from an implicit Newtonian dynamics. Analogies with classical mechanics are deeply ingrained within both modern economics and technical analysis. Absence of fundamental equations makes the task of building any statistical or quantum mechanics of market process extremely difficult, if possible. Nevertheless, based on symmetry, we are able to formulate probabilistic market dynamics, or a Gibbsian-like statistical market mechanics, by starting from this Newtonian-like representation (2). As already mentioned, the expression (2) is a convenient point of departure but other parameterizations are possible as long as they capture the two fundamental quantities v and g .

The representation of the price sequence $S(t_0), S(t_1), \dots, S(t_N)$ by (2) filters out the high-frequency variations of the price around the trend and its variation. This natural filter is usually performed to get rid as much as possible of the noise decorating such trend and acceleration. It is important to stress that the real price quotes $S(t_i)$ carry a lot of “noise” and not only information. Using a mean-square fit assumes that the residuals are Gaussian noise and implies that the coefficients A_0, A_1, A_2 are linearly dependent on the quoted prices $S(t_0), S(t_1), \dots, S(t_N)$. As we will show, this guarantees scaling invariance of the theory. For negative accelerations $A_2 < 0$, the model price $S_0(t)$ given by (2) is *not positively defined* for arbitrarily large future times, in contradiction with our above requirement. It is thus forbidden to use it directly for an extrapolation. However, we will show how it can be exploited extensively as a source of both qualitative and quantitative information about the future evolution of the market. In fact, the “bare” model price $S_0(t)$ can be used for qualitative predictions of the direction of the price movements, leaving aside magnitude of the moves.

We rewrite S_0 using a dimensionless time, so that it becomes explicit that S_0 remains invariant with respect to change of time units

$$S_0(T, F) = A_0(1 + T + F^{-1}T^2) , \quad (3)$$

where T is the dimensionless “reduced” time,

$$T = \frac{A_1}{A_0} t , \quad (4)$$

whose sign follows that of the velocity A_1 . The expression (3) is invariant with respect to a change of time units, since the coefficients A_p are transformed into $k^{-p} A_p$ under the transformation $t \rightarrow kt$. Due to this invariance, it is convenient to think of the beginning of the time series T_0 as the origin of time $T_0 = 0$ and take the last known time (present) T_N accordingly. The dimensionless Froude number F measures the relative strength of the price velocity A_1 compared to the price acceleration A_2 , given the price level A_0 attained at time 0:

$$F = \frac{A_1^2}{A_2 A_0} . \quad (5)$$

The sign of F is determined uniquely by that of the acceleration A_2 . This dimensionless ratio (5) is well-known in hydrodynamics as the *Froude* number. In the hydrodynamical context, this dimensionless number relates the ratio of inertia to buoyancy forces and is

applicable in particular to homogeneous shallow water flow, or two layers flow. Explicitly, in the shallow water approximation, the Froude number is $F = U^2/(gH)$, in which U is the characteristic velocity, H the characteristic fluid depth and g the acceleration due to gravity. Rather than an analogy with hydrodynamic turbulence [10] controlled by the Reynolds number weighting the nonlinear convective forces against the viscous forces, this analogy with gravity-controlled viscousless fluids is very suggestive: for viscousless liquids flowing above obstacles, two regimes can occur. (i) For Froude numbers remaining always less than one, the flow is only weakly perturbed by the obstacle. (ii) When the Froude number reaches one at some point above the obstacle, a major perturbation of the flow appears with a so-called hydraulic jump [12]. We will show below that similar regime transitions occur in the dynamics of market price as a function of the Froude number (5). The phenomenology of the market patterns is however significantly richer due to the importance of the signs of both A_1 and A_2 .

B. Functional Self-similarity and probabilistic scenarii

For each present time, we obtain a parabolic parameterization (3) that provides a robust coarse-grained representation of the information of past time prices. In principle, we may use much higher order polynomials or different nonlinear functions to represent more accurately the many degrees of freedom of the market price dynamics and then use these representation to extrapolate into the future. After initial optimism, this dynamical system approach [11,24] does not live up to expectations [21]. In addition, there are important technical problems in specifying high-order nonlinearities from noisy stock market data [11].

In contrast, we view the parabolic parameterization (3) as the unique projection of a large set of possible equivalent trajectories over the learning time interval $0 \leq T \leq T_N$. Only one of them will be selected by the dynamical evolution in the future. In order to construct this set of trajectories that allow for multiple scenarii, we view the parabolic parameterization (3) as the lowest order expansion *in the space of functions* containing more complicated functional forms, i.e. scenarii for the future. Our approach amounts to map the extrapolation in the future onto an evolution in the space of functions on increasingly complex “approximants” (scenarii) $y_n(t)$, which are linked to each other by the symmetry of functional self-similarity. This approach is very natural since the future evolution can always be encoded by some mathematical representation; the challenge is then to guess how to restrict the set of such representations to achieve predictability.

The symmetry of functional self-similarity allows us to reach this goal by the condition that different functions (scenarii) are not completely independent from each other but can be seen as constituting a hierarchical construction or multishell structure, such that the successive layers (approximations) $y_n(t)$, for $n = 0, 1, \dots$, are viewed as ordered realizations of a dynamical system evolving with respect to the approximation number n playing the role of an effective time in the functional space. The symmetry of functional self-similarity is expressed mathematically by self-similar renormalization group equations acting on the approximants: [26]

$$y_{n+m}(\varphi) = y_n(y_m(\varphi)) , \quad (6)$$

where all approximations are expressed as a function of a zeroth-order-approximation, through the relationship $y_0(t) \equiv \varphi$. In words, this property (6) of functional self-similarity means that the same functional relationship relates the approximant of order $n - 1$ to the approximant of order n as the approximant of order n to the approximant of order $n + 1$. The relation (6) expresses that all approximations are connected by an identical iteration procedure of successive improved approximations. This property also ensures the fastest convergence criterion [26], i.e. the strongest stability for the selected scenarii. Going from the abstract space of approximations to the real time, we thus obtain a set of self-similar extrapolation functions, corresponding to the different possible future market dynamics.

Using the dimensionless variables T and F and following the general procedure of algebraic self-similar bootstrap [26] recalled in the appendix, we deduce from the polynomial (3) the three simplest polynomial approximations

$$S_{00} = A_0, \quad S_{01} = A_0(1 + T), \quad S_{02} = A_0(1 + T + F^{-1}T^2) . \quad (7)$$

They correspond to successive truncations of (3) at increasing orders of the power of T . Implementing the algebraic self-similar bootstrap procedure [26] recalled in the appendix, we obtain two non-trivial approximants, which give two possible scenarii for the future price evolution:

$$S_1(T) = A_0 \exp(T) , \quad (8)$$

$$S_2(T, F) = A_0 \exp \left(T \exp \left(\frac{T}{F} \right) \right) . \quad (9)$$

Since T and F can be of both signs, $S_1(T)$ can be increasing or decreasing and $S_2(T)$ can be in addition non-monotonous.

These two scenarii-approximants (8,9) satisfy all symmetry demands formulated in section II. The approximant S_1 given by (8) is quite special since it possesses the self-similarity symmetry both in real time T and in the space of approximations. Indeed, a time translation leads solely to a redefinition of A_0 , while keeping exactly the same *functional* form. In contrast, the approximant S_2 is not invariant under a time translation and possesses only the functional self-similarity (6). It thus corresponds to a breaking of the time-translation symmetry.

The two scenarii-approximants (8,9) corresponds to two different forecasts for the future price evolution. What is the probability of each scenario? We follow ref. [27] and assume that the most probable scenario corresponds to the most stable approximant with respect to a change of the parabolic parameterization (3). In other words, the stability of each scenario is estimated by calculating the amplitude of its variation upon a change of the parameters of the parabolic parameterization (3). This allows us to use the concept of a Lyapunov exponent in the space of approximants. Then, using ideas from dynamical system theory, we generalize the dynamical Kolmogorov-Sinai entropy for the finite time behavior and stable as well as unstable trajectories. In our present context, the generalized Kolmogorov-Sinai entropy of an approximant is nothing else but the Lyapunov exponent associated to a variation of parabolic parameterization (3). As in [27], statistical physics then teaches us that a probability is obtained by taking the exponential $p \sim e^{-S}$ of minus the entropy and

then normalizing to one. Since the generalized Kolmogorov-Sinai entropy is nothing else but the entropy rate, it defines the entropy. Movement along a stable trajectory decreases the entropy counted from the entropy of the initial state, while the movement along an unstable trajectory increases the entropy. Probabilities are most conveniently expressed through the so-called multipliers, defined as the exponential of the Lyapunov exponents, and given by the functional derivative

$$m_k = \frac{\delta S_k}{\delta S_1}, \quad k = 1, 2. \quad (10)$$

which yields

$$m_1(T) = 1; \quad m_2(T, F) = \left(1 + \frac{T}{F}\right) \exp \left[T \left(\frac{1}{F} - 1 + \exp \left(\frac{T}{F} \right) \right) \right]. \quad (11)$$

The corresponding probabilities p_1 and p_2 for each scenario are inversely proportional to the multipliers and in proper normalization can be written as [27]

$$p_1(T, F) = \frac{1}{1 + |m_2(T, F)|^{-1}}, \quad p_2(T, F) = \frac{|m_2(T, F)|^{-1}}{1 + |m_2(T, F)|^{-1}}. \quad (12)$$

We define the average of the two scenerios as

$$S^*(T, F) = p_1(T, F) S_1(T) + p_2(T, F) S_2(T, F). \quad (13)$$

Probabilities defined in this way put more weight onto the trajectories with small multipliers which are the most stable, while not forbidding completely unstable trajectories with multipliers larger than one. One can imagine situations where all trajectories are unstable or neutral, with multiplier equal to or larger than 1. Then, the least unstable trajectory will receive more weight than the more unstable ones.

IV. CLASSIFICATION OF MARKET PHASES

The classification of market patterns depends on three parameters:

- the dimensionless time horizon $\Delta T/T_N$ normalized by the time interval T_N over which the parabolic representation is constructed,
- the reduced dimensionless learning period T_N itself,
- the Froude number F .

In order to classify the different possible temporal patterns of market prices, one should in principle compare the forecasted value $S^*(T_N + \Delta T, F)$ to the “present” price approximated by $S_0(T_N, F)$, where T_N and ΔT are the dimensionless times obtained from t_N and Δt by the transformation (4). We propose to use the average scenario $S^*(T, F)$ instead of $S_0(T_N, F)$ in order to reduce or eliminate as much as possible any systematic errors. Indeed, the use of the same function $S^*(T, F)$ provides a scheme for cancellation of errors that would not otherwise occur if the the parabola $S_0(T_N)$ given by (2) was chosen instead.

A given market pattern is thus determined by the behavior of the predicted return

$$R = \ln \left(\frac{S^*(T_N + \Delta T, F)}{S^*(T_N, F)} \right) . \quad (14)$$

We classify the different regimes by looking at the sign of the return and the transition between two regimes is quantified by the condition $R = 0$ which is equivalent to

$$\Delta S^* = S^*(T_N + \Delta T, F) - S^*(T_N, F) = 0 . \quad (15)$$

The number of solutions of equation (15) can be 0, 1, 2 or 3.

The following four combinations of the parameters are possible and define the following four regimes.

1. “Super-bull” ($\Delta T > 0, F > 0$) corresponding to positive price velocity and positive acceleration; we depict this regime with the following pictograph \downarrow .
2. “balanced-bull” ($\Delta T > 0, F < 0$) corresponding to positive price velocity and negative acceleration; we depict this regime with the following pictograph \uparrow .
3. “Super-bear” ($\Delta T < 0, F < 0$) corresponding to negative price velocity and negative acceleration; we depict this regime with the following pictograph \downarrow .
4. “Balanced-bear” ($\Delta T < 0, F > 0$) corresponding to negative price velocity and positive acceleration; we depict this regime with the following pictograph \uparrow .

In each case, one will find qualitatively different diagrams for the returns. A “Bull” regime of evolution corresponding to $R > 0$ will intermingle with a “Bear” regime corresponding to $R < 0$ in the phase space of control parameters in a way peculiar to each of the four cases.

Figure 1-6 presents some general statistics obtained from this classification. We have analyzed daily returns of twelve data sets comprising some major indices

- the Dow Jones index from Jan. 2, 1970 till Feb. 24, 1998,
- the SP500 index from Jan. 1, 1950 till June 1, 1999,
- the Nasdaq index from Feb. 5, 1971 till May 18, 1999,
- the German DAX index from July 1, 1991 till May 17, 1999,
- the British FTSE index from April 17, 1990 till May 17, 1999, and
- the Japanese Nikkei index from April 16, 1990 till May 17, 1999,

some major bonds

- the thirty year US treasury bond TYX from Oct. 29, 1993 till Aug. 9, 1999,
- the Japanese Government Bond JGB from Jan. 1, 1992 till March 23, 1999

and some major currencies against the US dollar all from Jan. 4, 1971 till May 19, 1999,

- the British pound GBP,
- the Swiss franc,
- the German mark,
- the Japanese Yen.

Each figure in the series 1-6 presents first the time evolution of the price (top). The middle plots represents the Froude number defined in equation (5) as a function of the reduced prediction horizon $\Delta T \equiv (A_1/A_0)\delta t$, where δt is fixed equal to 5 days. The four quadrants sampled clockwise correspond to the four regimes \rfloor , \lceil , \rceil and \lfloor defined above. The bottom plots quantify the relative frequency of each regime. Specifically, for each regime, we look at the sign of the return prediction and count the number of time a given regime with a given return sign has been predicted. In this way, we define eight patterns of which six fundamental ones remain to be considered by looking successively clockwise at the quadrants of the diagram of the Froude as a function of δT :

- $p_1 \equiv \rfloor+$: super bull predicting a positive return,
- $p_2 \equiv \rfloor-$: super bull predicting a negative return (impossible)
- $p_3 \equiv \lceil+$: balanced-bull predicting a positive return,
- $p_4 \equiv \lceil-$: balanced-bull predicting a negative return,
- $p_5 \equiv \rceil+$: super bear predicting a positive return (impossible)
- $p_6 \equiv \rceil-$: super bear predicting a negative return,
- $p_7 \equiv \lfloor+$: balanced-bear predicting a positive return,
- $p_8 \equiv \lfloor-$: balanced-bear predicting a negative return.

Note that $p_1 \equiv \rfloor+$, $p_3 \equiv \lceil+$, $p_6 \equiv \rceil-$ and $p_8 \equiv \lfloor-$ are trend-following patterns while $p_2 \equiv \rfloor-$, $p_4 \equiv \lceil-$, $p_5 \equiv \rceil+$ and $p_7 \equiv \lfloor+$ are contrarian patterns. Of these four contrarian patterns, only $p_4 \equiv \lceil-$ and $p_7 \equiv \lfloor+$ are allowed within the super-exponential framework. The theory thus accounts for a natural preferential bias in favor of trend-following patterns, while contrarian patterns do appear with non-negligible frequency.

The three dotted, dashed and continuous lines represent the transition between different signs of predicted returns from the condition (15): above (resp. below) the dotted line in the second (resp. third) quadrant, the predicted return is negative. It then turns positive between the dotted and dashed line, then negative again between the dashed and the continuous line and positive below (resp. above) the continuous line in the second (resp. third) quadrant.

Since market noise is an important issue, we also investigate how robust is a given pattern with respect to the amplitude of the predicted return: we count only those patterns with a predicted amplitude of the price variations ΔS^* defined by (15) larger than a threshold

defined as a multiple of the standard deviation of the fit of the price by the parabola $S_0(T_N)$ given by (2) in the training window of length t_N . The result is presented in the plots at the bottom of figures 1-6 showing the number of realizations of each of the six relevant patterns as a function of the threshold. When the threshold increases, some predictions are left over since their predicted price variation is below the threshold: we thus expect that the number of realizations of each pattern should decay as the threshold increases. We observe that the relative frequency of a given pattern decays typically exponentially with the threshold, in agreement with the approximate exponential character of the distribution of daily price variations [17] and of drawdowns [14,15]. Furthermore, among all patterns, the balanced-bull predicting negative returns ($p_4 \equiv \lceil -$) and balanced-bear predicting positive returns occur less frequently than the other patterns, showing a preponderance for trend-following patterns.

A. Super-bull \rfloor ($\Delta T > 0$, $F > 0$)

We start by a word of caution as this scenario is rather unstable. Indeed, In this case of positive dimensionless time and Froude number, the multiplier $m_2(T, F)$ is always larger than one, which means that the second scenario $S_2(T, F)$ is always unstable. When the Froude number decreases, both $m_2(T, F)$ and $S_2(T, F)$ grow larger and larger, becoming very large for sufficiently small F . However, the mathematical divergence only occurs at infinite times. Strickly speaking, this does not violate the principle requested by our theory that price remaining finite; however, in practice, it may lead to instabilities. The formal definition of the finite average S^* still holds mathematically speaking but the accuracy may be problematic. Limiting the theory to a second-order regression (i.e. solely in terms of the velocity and the acceleration) is a limiting feature of our present approach and should be improved by considering higher-order approximants.

In the super-bull case, the prediction is that returns are expected to be always positive corresponding to pattern $p_1 \equiv \rfloor +$.

Figure 7,8 presents statistical tests of this prediction on the twelve data sets shown in figures 1-6. In these plots, the learning interval is fixed to 15 days and the prediction horizon is fixed to 5 days. For each asset, two plots are presented. The top one shows the normalized number of successes for the prediction of the sign of the return as a function of threshold, where the threshold is defined as in figures 1-6. A normalized success close to 0.5 corresponds to a 50% probability of being right or wrong and is thus undistinguishable from chance. The issue however is more subtle because the existence of trends in certain markets such as in indices bias this estimation. To account for such bias and others stemming from specific structures of the distributions of daily returns in the raw time series, we have generated 1000 surrogate times series for each of the 12 assets by reshuffling at random the daily returns. On each of the 1000 surrogate time series, we have applied our procedure and have measured the success rate as a function of threshold, following the same methodology as for each initial time series. This allows us to plot the 90% (continuous line) and 99% (dotted line) confidence levels, defined by the fact that 900 (resp. 990) among the 1000 surrogate times series gave a success rate in the interior of the domain bounded by the continuous (resp. dotted) line.

In addition, since our framework incorporate both a trend-following component (quantified by the velocity) and contrarian ingredient (quantified by the acceleration), it is instructive to compare its performance with two strategies.

1. The first one is a simple trend-following strategy and consists of taking the linear approximation $A_0(1+T) = A_0 + A_1t$ of the simple exponential approximant S_1 as the best prediction. This strategy is independent of the acceleration A_2 and is thus a pure trend-following strategy: it rises (resp. decreases) if the velocity A_1 is positive (resp. negative).
2. The second strategy consists in using the bare parabolic parameterization (3), which represents the best representation of the local market behavior incorporating the interplay between trend and acceleration without any theoretical improvement.

In this way, we can really quantify the value, if any, brought by our theory, compared to more traditional technical analysis methods.

The bottom plot for each asset in figure 7,8 gives the normalized number of times the pattern has been found as a function of the threshold, this for the three different strategies, namely our best prediction based on the average S^* over the two approximants, the trend-following strategy (linear approximation of S_1) and the parabolic parameterization (3). This plot is important in order to assess the quantitative importance of a given success rate in terms of its frequency. Consider for instance the Swiss franc. We observe that both the trend and average approximant exhibit statistically significant predictive power with two notable peaks as a function of threshold, approximately at 0.5 and 1.2, with a success rate approaching 60% in the first case and overpassing 80% in the second case. The apparent overwhelming superiority of the second peak is moderated by the fact that it concerns about 1/10th of the cases covered by the first peak for the average approximant and about 1/100th of the case covered by the first peak for the trend-following strategy. Their impact for a successive investment strategy will thus be an interplay between their success rate and the occurrence rate.

The following overall picture emerges from examination of the twelve markets shown in figure 7,8. Taken together, we find that the trend-following and the average approximant strategies exhibit statistically significant success rates, while the parabolic strategy is not different from random coin tossing. While the trend-following strategy seems to exhibit sometimes a better performance than the average approximant, it is much less robust in terms of its number of occurrences.

B. Balanced-Bull market [$(\Delta T > 0, F < 0)$]

In the balanced-bull regime, both positive and negative returns can be predicted. A “phase diagram”, defined in the parameter space $(\Delta T/T_N, |F|)$ with $T_N = 1$ and shown in figure 9, summarizes the different possible cases. From the condition of positive prices $S_0 > 0$, we find that F must satisfy the condition

$$|F| > F_0 = \frac{T_N^2}{1 + T_N} .$$

There are three branches that solve equation (15): $F_1(\Delta T)$, $F_2(\Delta T)$ and $F_3(\Delta T)$, with $|F_1(\Delta T)| < |F_2(\Delta T)| < |F_3(\Delta T)|$. These curves are shown in figure 9 as dotted-dashed, dashed and continuous lines respectively. Below the curve $|F_1(\Delta T)|$, R is always negative, corresponding to a trend-reversing forecast for all possible time horizons, while R becomes positive above the curve, corresponding to the trend-following forecast for large $|F|$. There is also a “tongue”-shaped region of trend-reversing regime, encircled by the curves $|F_2(\Delta T)|$ and $|F_3(\Delta T)|$. We are inclined to interpret this region as an artifact appearing as a remnant of the non-renormalized phase-equilibria curve.

It is instructive to calculate the line delineating the change of sign of the return, which would follow directly from the non-renormalized price S_0 , given by the condition $S_0(T_N + \Delta T, F) - S_0(T_N, F) = 0$, and compare it to the phase-equilibria for the renormalized price. This line is shown in figure 9 as the long-dashed line and is referred to as “regression”.

These results can be understood intuitively as follows. A small absolute value of the Froude number implies a large (negative) acceleration, hence the possibility for the price to change course over the prediction horizon. We thus expect and observe that the predicted return is negative *below* a transition line, both for the non-renormalized price parabola S_0 and for our prediction S^* . We observe that the effect of the functional renormalization is to shift significantly the transition line towards lower $|F|$, i.e. larger negative accelerations. This can be seen to result in part from the stabilization effect of the positivity property of super-exponentials.

We note that these results are robust with respect to a change of the dimensionless learning period T_N , which has only a marginal influence only on the quantitative shape of the phase diagram but not on its qualitative properties. In fact, the topological properties of the transition lines never change when varying T_N .

Figure 10 shows the predicted return defined by equation (14) as a function of the ratio $\Delta T/T_N$ of the prediction horizon over the learning interval for several values of the Froude number. The three boundaries $F_1(\Delta T)$, $F_2(\Delta T)$ and $F_3(\Delta T)$ shown in figure 9 can be deduced qualitatively from this figure 10 from the three regimes where R is always positive (large $|F|$), R changes signs with a cusp (intermediate $|F|$) and is always negative (small $|F|$).

These predictions are tested in figure 11,12,13,14 which presents statistical tests on the twelve data sets shown in figures 1-6. The same parameters as for the super bull regime tested in figure 7,8 have been used (the learning interval is fixed to 15 days and the prediction horizon is fixed to 5 days).

Pattern 3 corresponding to the trend-following pattern $\lceil +$ is first shown. We observe that the parabolic prediction (open circles) and the average approximant (crosses) strategies exhibit statistically significant success rates, while the trend-following strategy is not different from random coin tossing. While the parabolic prediction strategy seems to exhibit sometimes a better performance than the average approximant, it is much less robust in terms of its number of occurrences.

For pattern 4 corresponding to the contrarian pattern $\lceil -$, we show only two strategies, the average approximant (crosses) and the bare parabolic parameterization (3) represented by open circles, since the trend-following strategy never predicts the pattern $\lceil -$ by definition. The average approximant clearly exhibits statistically significant success rates for most of

the assets, while the parabolic strategy is not different from random coin tossing in this explored threshold range.

C. Super-bear \rfloor ($\Delta T < 0, F < 0$)

We start by a word of caution as this scenario is rather unstable. In this case of negative dimensionless time and Froude number, the multiplier $m_2(T, F)$ and its associated scenario $S_2(T, F)$ both go to very small values with decreasing $|F|$ in the limit of small $|F|$. The average approximant S^* goes to zero as well. The large variations are symptomatic of potential instabilities. Limiting the theory to a second-order regression (i.e. solely in terms of the velocity and the acceleration) is a limiting feature of our present approach for the super-bear (as it was the case for the super-bear discussed above) and should be improved by considering higher-order approximants.

In the super-bear case, the prediction is that returns are expected to be always negative corresponding to pattern $p_6 \equiv \rfloor -$. Pattern $p_7 \equiv \rfloor +$ is thus impossible within the present framework limited to a characterization of the market price evolution solely in terms of a velocity and an acceleration.

Figure 15,16 presents the same statistical tests as in figure 7,8 of this prediction on the twelve data sets shown in figures 1-6. In these plots, the learning interval is fixed to 15 days and the prediction horizon is fixed to 5 days. As for the super-bull case, we observe that the trend-following and the average approximant strategies exhibit statistically significant success rates, while the parabolic strategy is not different from random coin tossing. While the trend-following strategy seems to exhibit sometimes a better performance than the average approximant, it is much less robust in terms of its number of occurrences.

D. Balanced-Bear \lfloor ($\Delta T < 0, F > 0$)

In the balanced-bear regime as for the previously discussed balanced-bull regime, both positive and negative returns can be predicted. A “phase diagram”, defined in the parameter space $(\Delta T/T_N, |F|)$ with $T_N = 1$ and shown in figure 17, summarizes the different possible cases.

There are three branches that solve equation (15): $F_1(\Delta T)$, $F_2(\Delta T)$ and $F_3(\Delta T)$, with $F_1(\Delta T) < F_2(\Delta T) < F_3(\Delta T)$. The phase diagram shown in figure 17 looks very similar to the balanced-bull case, with the region of positive (resp. negative) returns below (resp. above) the $F_1(\Delta T)$ curve. There is again a “tongue”-shaped region of trend-reversing regime, encircled by the curves $F_2(\Delta T)$ and $F_3(\Delta T)$. We propose to interpret this region as an artifact appearing as a remnant of the non-renormalized phase-equilibria curve. We show in addition the line of change of sign for the return predicted by the non-renormalized price S_0 , given by the condition $S_0(T_N + \Delta T, F) - S_0(T_N, F) = 0$.

For small F , the average approximant S^* as well as the non-renormalized parabolic parameterization S_0 both predict a trend-reversing regime. The interpretation is the following: a small Froude number corresponds to a large positive acceleration, which has thus the capacity of reversing the negative trend over the prediction horizon. The main effect of our

renormalization procedure is to shift the transition line downwards to smaller Froude numbers, i.e. to larger accelerations, a result that derives from the stabilization of our procedure. This exemplifies the non-trivial nature of the scenarii selected by the self-similar functional renormalization group approach. For larger F , i.e. smaller accelerations, the trend-following forecast takes over.

The reduced dimensionless learning period T_N is again a marginally relevant parameter, i.e. it influences the shape of phase diagram only quantitatively. The shape and topology of the phase equilibria curves are similar for all T_N .

It is interesting to notice that our classification of possible market regimes exhibit a distinct asymmetry between bullish and bearish phases: a balanced-bull market and a balanced-bear market will not evolve symmetrically in time. Most significantly, the line of phase equilibria for the balanced-bear case saturates at large $\Delta T/T_N$ at some constant value which is function only of T_N , while for the balanced-bull case there is no such saturation.

Figure 18 shows the predicted return R defined by equation (14) as a function of the ratio $\Delta T/T_N$ of the prediction horizon over the learning interval for several values of the Froude number. The three boundaries $F_1(\Delta T)$, $F_2(\Delta T)$ and $F_3(\Delta T)$ shown in figure 17 can be deduced qualitatively from this figure 18 from the three regimes where R is always positive (small F), R changes signs with a cusp (intermediate F) and is always negative (large F).

These predictions are tested in figure 19,20,21,22 which presents statistical tests on the twelve data sets shown in figures 1-6. The same parameters as for the super bull regime tested in figure 7,8 have been used (the learning interval is fixed to 15 days and the prediction horizon is fixed to 5 days).

Pattern 7 corresponding to the trend-reversal or contrarian pattern $\lfloor +$ is first shown. Only two strategies are shown, namely the average approximant (crosses) and the bare parabolic parameterization (3) represented by open circles, since the trend-following strategy never predicts the pattern $\lfloor +$ by definition. The average approximant clearly exhibits statistically significant success rates for most of the assets, while the parabolic strategy is not different from random coin tossing.

For pattern 8 corresponding to the trend-following case $\lfloor -$, we observe that the parabolic prediction (open circles) and the average approximant (crosses) strategies exhibit statistically significant success rates, while the trend-following strategy is not different from random coin tossing. While the parabolic prediction strategy seems to exhibit sometimes a better performance than the average approximant, it is much less robust in terms of its number of occurrences.

V. DISCUSSION AND CONCLUSION

In summary, we have presented a general framework that characterizes different market phases viewed as local defects of the overall time-translational invariance structure of the random walk reference. This framework is based on the price velocity and acceleration parameters and on a set of symmetry principles, especially self-similarity of the prices and in the abstract space of functional scenarii.

We have tested the quality of the predictions provided by our theory by measuring the success rate of the prediction of the sign of the return on twelve different assets and have

compared the quality of these predictions to those from for traditional technical analysis including a trend-following and a contrarian strategy. The statistical significance of our results have been assessed by generating 1000 surrogate time series for each of the twelve assets with exactly the same statistical properties except for possible time-dependence, by reshuffling the daily returns. The application of the three forecasting strategies to these 1000 surrogate times series shows that our predictive skill has overall a high degree of statistical significance. Furthermore, we find that it is robust over all phases of the market. This is in constrast with the trend-following strategy which is found to perform well only during strong accelerating trends (categorized as “super-bull” and “super-bear”). This is also in contrast with the contrarian strategy which is found to perform well only during decelerating trends (categorized as “balanced-bull” and “balanced-bear”). Our probabilistic framework thus provides an automatic scheme for detecting and selecting what type of strategy is the best performer. This optimization relies on the calculation of the stability of the different scenarii: the most stable one is the most probable and controls the strategy (trend-following or contrarian) that is best adapted to a particular phase of the market.

The present framework can be seen as a generalization of the standard “Newtonian” deterministic technical analysis to a Gibbsian (statistical) mechanics, in other words, to a probabilistic view of the future. The appearance of probabilities has to be emphasized in constrast to a deterministic view of future. This probabilistic framework captures the inhomogeneity of market participants who can produce different forecasts based on equivalent information. It may thus provide a forum for reconciliation of the on-going feud between “efficient marketers” and “technicians”, by showing that the random walk paradigm and a determinism view of the world are different limiting cases of much broader and complex market evolutions.

Acknowledgements: We are grateful to D. Darcet, A. Johansen and V.I. Yukalov for stimulating discussions.

APPENDIX: STATISTICAL SELF-SIMILAR ANALYSIS

In this appendix, we recall the theory that leads to the results quoted in section IIIB. We look at the prediction of the future time evolution of the market as a specification of an a priori unknown function $f(x)$ of a real variable x representing the fundamental market trajectory as a function of physical time or the dimensionless time. We keep the notation $f(x)$ to be general.

The first step of the theory consists in recognizing that, in the neighborhood of the present time $x = x_0$, one can define a series of approximations $p_k(x, x_0)$ (also called asymptotic expansions) to this function with $k = 0, 1, 2, \dots$:

$$f(x) \simeq p_k(x, x_0), \quad x \rightarrow x_0. \quad (16)$$

The number k indexes the order of the approximations obtained according to some construction scheme, which can be convergent or divergent (i.e. asymptotic).

Following the algebraic self-similar renormalization procedure [26], one introduces the algebraic transform defined by

$$P_k(x, s, x_0) = x^s p_k(x, x_0), \quad (17)$$

where the exponent s is yet unknown, and later will play the role of a control function. The inverse transform to that in Eq.(17) is

$$p_k(x, x_0) = x^{-s} P_k(x, s, x_0). \quad (18)$$

The introduction of the transform (17) in terms of power law products keeps the symmetry requirements discussed in the main text and offers an additional degree of freedom in the space of functions to impose positivity and get rid of infinities (poles). Rather than constructing a trajectory in the space of the initial approximations, the idea behind the introduction of the transform (17) is to deform smoothly the initial functional space of the approximations $p_k(x, x_0)$ in order to obtain a faster and better controlled convergence in the space of the modified functions $P_k(x, s, x_0)$. This convergence can then be mapped back to get the relevant estimations and predictions.

Technically, the procedure is as follows [26]. One first defines an expansion function $x = x(\varphi, s, x_0)$ by the equation

$$P_0(x, s, x_0) = \varphi, \quad x = x(\varphi, s, x_0), \quad (19)$$

where P_0 is the first available term from the sequence $\{P_k\}$. This allows one to transform the problem of searching for an approximation as a function of time into the problem of the dependence of the time as a function of the first approximant. This type of transformation is well-known and a closely related one is for instance used in hydrodynamics under the name of the hodograph transform to solve very non-linear flow problem [6] that are otherwise out of reach of standard functional methods. The variable φ represents the running and continuous interpolation between successive approximations in the space of functions.

Once this change of variable is performed, all functions can be expressed in terms of this new variable φ , which defines

$$y_k(\varphi, s, x_0) = P_k(x(\varphi, s, x_0), s, x_0) . \quad (20)$$

The transformation inverse to Eq. (20) reads

$$P_k(x, s, x_0) = y_k(P_0(x, s, x_0), s, x_0) . \quad (21)$$

The family of endomorphisms, $\{y_k\}$, allows to define the “velocity” field

$$v_k(\varphi, s, x_0) = y_{k+1}(\varphi, s, x_0) - y_k(\varphi, s, x_0) , \quad (22)$$

corresponding to the change of the approximants per unit order of the approximations. The trajectory of the sequence $\{y_k\}$ is, by definitions (20) and (21), bijective to the approximation sequence $\{P_k\}$.

From the knowledge of the velocity as a function of the variable φ , one defines an effective time increment τ for the evolution of the dynamical system in the space of functions: during that time increment τ , P_k is transformed into P_{k+1} . This provides the evolution integral

$$\int_{P_k}^{P_{k+1}^*} \frac{d\varphi}{v_k(\varphi, s, x_0)} = \tau , \quad (23)$$

in which $P_k = P_k(x, s, x_0)$ is any given term from the approximation sequence $\{P_k\}$; $P_{k+1}^* = P_{k+1}^*(x, s, \tau, x_0)$ is the best guess obtained in this approach for the fixed point of the approximation series. τ is an effective minimal time necessary for reaching this fixed point.

Recall that we started with a sequence $\{p_k\}$ of asymptotic expansions of the function $f(x)$. We then passed to the sequence $\{P_k\}$ by means of the algebraic transformation (17). We now have to return back by employing the inverse transformation (18). To this end, we set

$$F_k^*(x, s, \tau, x_0) = x^{-s} P_k^*(x, s, \tau, x_0) . \quad (24)$$

The quantities s and τ are the control functions guarantying the stability of the method, that is, the convergence of the procedure. These functions are to be defined by the stability conditions, such as the minimum of multiplier moduli, together with additional constraints, like, e.g., boundary conditions. Let us assume that we find from such conditions $s = s_k$ and $\tau = \tau_k$. Substituting these into Eq.(24), we obtain the self-similar approximation

$$f_k^*(x, x_0) = F_k^*(x, s_k, \tau_k, x_0) \quad (25)$$

for the function $f(x)$.

Let us now apply this theory to the polynomial perturbative series

$$p_k(x) = \sum_{n=0}^k a_n x^n, \quad a_0 \neq 0 , \quad (26)$$

containing integer powers of x as in (2). Then, the algebraic transform (17) reads

$$P_k(x, s) = \sum_{n=0}^k a_n x^{n+s} . \quad (27)$$

The transform (27) corresponds to an effective higher perturbation order $k + s$, as compared to the initial series (26) of order k . Eq.(19) for the expansion function $x(\varphi, s)$ now reads

$$P_0(x, s) = a_0 x^s = \varphi, \quad (28)$$

which yields

$$x(\varphi, s) = \left(\frac{\varphi}{a_0} \right)^{1/s}. \quad (29)$$

The series of functions (20) become

$$y_k(\varphi, s) = \sum_{n=0}^k a_n \left(\frac{\varphi}{a_0} \right)^{n/s+1}. \quad (30)$$

The velocity field (22) reads

$$v_k(\varphi, s) = a_k \left(\frac{\varphi}{a_0} \right)^{1+k/s}. \quad (31)$$

With the optimization condition $\tau = 1$ corresponding to the requirement that the fixed point is reached under a single iteration, the evolution integral (23) gives

$$P_k^*(x, s) = P_{k-1}(x, s) \left[1 - \frac{k a_k}{s a_0^{1+k/s}} P_{k-1}^{k/s}(x, s) \right]^{-s/k}. \quad (32)$$

The stabilizer $s_k(x)$ is determined from the minimization of the multiplier defined by

$$\mu_k(\varphi, s) = \frac{\partial}{\partial \varphi} y_k(\varphi, s), \quad (33)$$

which is then transformed into its image

$$m_k(x, s) = \mu_k(F_0(x, s), s) \quad (34)$$

in terms of the variable x , This yields

$$m_k(x, s) = \sum_{n=0}^k \frac{a_n}{a_0} \left(1 + \frac{n}{s} \right) x^n. \quad (35)$$

The control function $s = s_k(x)$ is defined by the equation

$$|m_k(x, s_k(x))| = \min_s |m_k(x, s)|. \quad (36)$$

Because the minimization of the multiplier $|m_k(x, s)|$ makes the trajectory in the space of functions more stable, the role of the control function $s_k(x)$ is now justified as a stabilizing tool. This provides finally the self similar approximation (25),

$$f_k^*(x) = p_{k-1}(x) \left[1 - \frac{k a_k}{s a_0^{1+k/s}} x^k p_{k-1}^{k/s}(x) \right]^{-s/k}, \quad (37)$$

where $s = s_k(x)$ is the solution of (36).

An interesting case occurs when the limit $s \rightarrow \infty$ is taken for which the approximants will be shown below to be super-exponentials, i.e. an exponential of an exponential of an exponential... This limit $s \rightarrow \infty$ often realizes the minimum of the multipliers (hence ensures the optimal convergence and stability of the procedure) and also corresponds to the maximum effective order of the perturbation expansion (27).

Note that this limit $s \rightarrow \infty$ does not always optimize the renormalization procedure at *every step*, i.e. does not always minimize the local multipliers; however, we find that the solutions are closed to this limit. In addition, we emphasize that the fastest convergence of the procedure at each step does not guarantee that the final expression will converge to the true fixed point. Quite often, one can find already at the very first steps of the renormalization that some multipliers vanish, which mathematically would mean an infinite rate of convergence, while in practice this makes the procedure trapped close to a wrong fixed point. It is better to look at the optimal stability criterion from a global perspective, i.e. over several steps of the renormalization. The particularly interesting properties shared by the solutions of the limit $s \rightarrow \infty$ are the following:

1. the super-exponentials are obtained under the condition where as many steps as possible are performed towards the sought fixed point. Furthermore, the total exponentiation is the strongest possible way to renormalize initial power series.
2. The explicit self-similarity of the final super-exponential expressions and their iterative nature allows us to look at them in turn as a sequence of approximations to the fixed point and compare their quality with respect to the lowest-order exponential by means of the “global” multipliers. In general, super-exponentials surround the fixed point, but do not hit it precisely.
3. For massive numerical calculations it is convenient to have fixed and reasonable functional forms for the approximants rather than define them at each step, as step-by-step renormalization would require.

Taking this limit $s \rightarrow \infty$ in (37) gives

$$f_k^*(x) = p_{k-1}(x) \exp\left(\frac{a_k}{a_0} x^k\right). \quad (38)$$

Repeating the renormalization, we get

$$f_k^{**}(x) = p_{k-2}(x) \exp\left\{\frac{1}{a_0}(a_{k-1}x^{k-1} + a_k x^k)\right\}. \quad (39)$$

Iterating the procedure, we obtain the k -fold approximation (36) in the form

$$f_k^{***}(x) = a_0 \exp\left\{\frac{1}{a_0}(a_1 x + a_2 x^2 + \dots + a_k x^k)\right\}. \quad (40)$$

We see that the k -th approximation (40) is expressed through a part of the initial perturbation series (26), namely, through

$$p_k(x) - a_0 = \sum_{n=1}^k a_n x^n.$$

With the notation

$$p'_k(x) \equiv \sum_{n=0}^k a'_n x^n , \quad (41)$$

in which $a'_n \equiv a_{n+1}$, $n = 0, 1; 2, \dots, k$, we may rewrite (40) as

$$f_k^{*\dots*}(x) = a_0 \exp\left\{\frac{x}{a_0} p'_{k-1}(x)\right\} . \quad (42)$$

The same functional renormalization procedure can now be applied to the power series $p'_{k-1}(x)$, giving the corresponding self-similar approximation

$$f'_{k-1}(x) = a'_0 \exp\left\{\frac{x}{a'_0} p''_{k-2}(x)\right\} , \quad (43)$$

in which

$$p''_k(x) \equiv \sum_{n=0}^k a''_n x^n, \quad a''_n \equiv a_{n+2} . \quad (44)$$

With this renormalization, we transform (42) into

$$f_k^{*\dots*}(x) = a_0 \exp\left\{\frac{x}{a_0} f'_{k-1}(x)\right\} . \quad (45)$$

Combining (43) and (45), we have

$$f_k^{*\dots*}(x) = a_0 \exp\left\{\frac{x}{a_0} a_1 \exp\left\{\frac{x}{a_1} p''_{k-2}(x)\right\}\right\} . \quad (46)$$

Converting k times all power series in the exponentials, with the use of the notation

$$b_0 = a_0 , \quad b_k = \frac{a_k}{a_{k-1}} , \quad k = 1, 2, \dots, \quad (47)$$

we obtain the *bootstrap self-similar approximation*

$$\widetilde{f}_k(x) = b_0 \exp(b_1 x \exp(b_2 x \exp(\dots b_{k-1} x \exp(b_k x)) \dots)) , \quad (48)$$

introduced by Yukalov and Gluzman [28]. It is this fundamental result that we use to obtain expressions (8) and (9) in the main text.

REFERENCES

- [1] S.B. Achelis, Technical Analysis, From A to Z, Irwin (1995)
- [2] W.B. Arthur, Y.M. Ermoliev and Y.M. Kaniovski, Path-Dependent Processes and the Emergence of Macro-Structure, *European Journal of Operational Research* 30, 294-303 (1987).
- [3] W.B. Arthur, Complexity and the economy, *Science* 284, N5411:107-109 (1999); W. B. Arthur, J. H. Holland, B. LeBaron, R. G. Palmer and P. Tayler, Asset pricing Under Endogenous Expectations in an Artificial Stock Market, in *The Economy as a Complex Adaptive System II*, Edited by W. Brian Arthur et al. , Reading, Addison-Wesley (1997); R.G. Palmer, W.B. Arthur, J.H. Holland, B. LeBaron and P. Tayler, Artificial economic life - A simple model of a stock market, *Physica D* 75, 264-274 (1994); G. Caldarelli, M. Marsili and Y.C. Zhang, A prototype model of stock exchange, *Europhysics Letters* 40, 479-484 (1997).
- [4] I. Asimov, Isaac, Foundation, 1st Ballantine Books ed. New York : Ballantine Books (1983); *The Foundation trilogy : three classics of science fiction*, Garden City, N.Y. : Doubleday (1982).
- [5] R.J. Bauer and J.R. Dahlquist, *Technical Market Indicators, Analysis and Performance*, J. Wiley, New York, 1999.
- [6] D. Bensimon, Kadanoff L.P., Liang S., Shraiman B.I. and Tang C., *Rev.Mod.Phys.* 58, 977 (1986)
- [7] W. Brock, J. Lakonishok and B. LeBaron, Simple Technical Trading Rules and the Stochastic Properties of Stock Returns, *Journal of Finance* 47, 1731-1764 (1992).
- [8] B. Dubrulle, F. Graner and D. Sornette, eds., *Scale invariance and beyond*, EDP Sciences and Springer, Berlin (1997).
- [9] J. D. Farmer, Market force, ecology and evolution, preprint adap-org/9812005
- [10] S. Ghashghaie, W. Breymann, J. Peinke, P. Talkner and Y. Dodge, Turbulent cascades in foreign exchange markets, *Nature* 381, 767-770 (1996); A. Arneodo, J.F. Muzy and D. Sornette, "Direct" causal cascade in the stock market, *European Physical Journal B* 2, 277-282 (1998).
- [11] J.F. Gibson, J.D. Farmer, M. Casdagli and S. Eubank, An analytic approach to practical state space reconstruction, *Physica D* 57, 1-30 (1992); M. Casdagli, S. Eubank, J.D. Farmer and J.F. Gibson, State space reconstruction in the presence of noise, *Physica D* 51, 52-98 (1991); J. Theiler, S. Eubank, A. Longtin, B. Galdrikian and J.D. Farmer, Testing for nonlinearity in time series – The method of surrogate data, *Physica D* 58, 77-94 (1992).
- [12] E. Guyon, J.-P. Hulin and L. Petit, *Hydrodynamique Physique*, Savoirs Actuels, InterEditions/Editions du CNRS, Paris (1994).
- [13] N. Jagadeesh, Evidence of predictable behavior of security returns, *Journal of Finance*, July, 881-898 (1990)
- [14] A. Johansen and D. Sornette, Stock market crashes are outliers, *European Physical Journal B* 1, 141-143 (1998)
- [15] A. Johansen and D. Sornette, Distributions of drawdowns, working paper (1999)
- [16] O.M. Joy, Should we believe the tests of market efficiency? *Journal of Portfolio Management*, summer, 49-54 (1986)
- [17] Jean Laherrère and Didier Sornette, Stretched exponential distributions in Nature and

- Economy: “Fat tails” with characteristic scales, *European Physical Journal B* 2, 525-539 (1998)
- [18] B.N. Lehmann, Fads, Martingales and Market Efficiency, *The Quarterly Journal of Economics*, February, 1-28 (1990)
 - [19] S.-K. Ma, *Statistical mechanics* (Philadelphia : World Scientific, 1985).
 - [20] J.A. Murphy, Futures fund performance: a test of the effectiveness of technical analysis, *Journal of Futures Markets*, Summer, 175-185 (1986)
 - [21] E.E. Peters, *Fractal market analysis : applying chaos theory to investment and economics*, New York : J. Wiley & Sons (1994).
 - [22] For a large collection of free technical analysis materials, see <http://decisionpoint.com/>
 - [23] P.A. Samuelson, *Collected Scientific Papers*, M.I.T. Press, Cambridge, MA (1972).
 - [24] J.A. Scheinkman and B. LeBaron, Nonlinear Dynamics and Stock Returns, *Journal of Business* 62, 311-337 (1989).
 - [25] D.A. Washburn and R.T. Putney, Stimulus movement and the intensity of attention, *Psychological Record* 48, 555-570 (1998); H. Braunstein Bercovitz and R.E. Lubow, Latent inhibition as a function of modulation of attention to the preexposed irrelevant stimulus, *Learning and Motivation* 29, 261-279 (1998); J. Musseler and G. Aschersleben, Localizing the first position of a moving stimulus: The Frohlich effect and an attention-shifting explanation, *Perception & Psychophysics* 60, 683-695 (1998); S.L. Hsieh, Stimulus-driven or autonomous shift of attention, *Perceptual and Motor Skills* 80, 1187-1199 (1995); D.A. Washburn, The stimulus movement effect – Allocation of attention or artifact, *Journal of Experimental Psychology- Animal Behavior Processes* 9, 380-390 (1993); K.M. Mohan, V. Dobson, E.M. Harvey, S.M. Delaney, and others, Does rate of stimulus presentation affect measured visual field extent in infants and toddlers? *Optometry and Vision Science* 76, 234-240 (1999); S.K. Fisher, K.J. Ciuffreda and J.E. Bird, The effect of stimulus duration on tonic accommodation and tonic vergence, *Optometry and Vision Science* 67, 441-449 (1990); S. Mattes and R. Ulrich, Directed attention prolongs the perceived duration of a brief stimulus, *Perception & Psychophysics* 60, 1305-1317 (1998).
 - [26] V. I. Yukalov, Method of self-similar approximations. *J. Math. Phys.* 32 (5), 1235-1239 (1991); V.I. Yukalov and S. Gluzman, Self-similar exponential approximants. *Phys. Rev. E* 58, 1359-1382 (1998); S. Gluzman and V.I Yukalov, Algebraic self-similar renormalization in the theory of critical phenomena. *Phys. Rev.* 55, 3983-3999 (1997).
 - [27] V. I. Yukalov and S. Gluzman, Weighted Fixed Points in Self-Similar Analysis of Time Series, *International Journal of Modern Physics B* 13, 1463 (1999).
 - [28] V.I. Yukalov and S. Gluzman, Self-similar bootstrap of divergent series, *Phys. Rev.* 55, 6552-6565 (1997).
 - [29] Y.-C. Zhang, Toward a Theory of Marginally Efficient Markets, preprint cond-mat/9901243

FIGURES

FIG. 1. US dollar in German mark and Japanese Yen from Jan. 4, 1971 till May 19, 1999. The plots at the top show the time series of the prices. The middle plots show the Froude number defined in equation (5) as a function of the reduced prediction horizon $\Delta T \equiv (A_1/A_0)\delta t$ where δt is fixed equal to 5 days. The plots at the bottom show the number of realizations of each of the six relevant patterns as a function of the threshold for the predicted amplitude of the price move. The symbols are $p_1 \equiv]+ (x)$, $p_3 \equiv [+ (+)$, $p_4 \equiv [- (o)$, $p_6 \equiv]- (.)$, $p_7 \equiv [+ (square)$ and $p_8 \equiv [- (diamond)$. The dotted, dashed and continuous lines delineate domains of different predicted return signs (see text).

FIG. 2. Same as figure 1 for the British pound and the Swiss franc.

FIG. 3. Same as figure 1 for the thirty year US treasury bond TYX from Oct. 29, 1993 till Aug. 9, 1999, and the Japanese Government Bond JGB from from Jan. 1, 1992 till March 23, 1999.

FIG. 4. Same as figure 1 for the SP500 index from Jan. 1, 1950 till June 1, 1999, and the Dow Jones index from Jan. 2, 1970 till Feb. 24, 1998.

FIG. 5. Same as figure 1 for the Nasdaq index from Feb. 5, 1971 till May 18, 1999, and the Japanese Nikkei index from April 16, 1990 till May 17, 1999.

FIG. 6. Same as figure 1 for the British FTSE index from April 17, 1990 till May 17, 1999, and the German DAX index from July 1, 1991 till May 17, 1999.

FIG. 7.

FIG. 8. Super bull case $] :$ comparative statistical tests of the predictions of our theory (average approximant S^*) represented by crosses, a trend following strategy (linear approximation of S_1) represented by open squares and the bare parabolic parameterization (3) represented by open circles, for the twelve assets presented in figure 1-6. For information on how the figures are constructed, see the main text.

FIG. 9. “Phase diagram” for the balanced-bull regime \lceil , defined in the parameter space $(\Delta T/T_N, |F|)$ with $T_N = 1$, delineating the regions of positive and negative returns. The boundaries $F_1(\Delta T)$, $F_2(\Delta T)$ and $F_3(\Delta T)$ are shown as dotted-dashed, dashed and continuous lines respectively. The long-dashed line indicated as “regression” on the figure corresponds to the solution of $S_0(T_N + \Delta T, F) - S_0(T_N, F) = 0$.

FIG. 10. Predicted return R in the balanced-bull regime \lceil defined by equation (14) as a function of the ratio $\Delta T/T_N$ of the prediction horizon over the learning interval for several values of the Froude number.

FIG. 11.

FIG. 12.

FIG. 13.

FIG. 14. Balanced bull case \lceil : Comparative statistical tests of the predictions of our theory (average approximant S^*) represented by crosses, a trend following strategy (linear approximation of S_1) represented by open squares and the bare parabolic parameterization (3) represented by open circles, for the twelve assets presented in figure 1-6. The predictions of positive $\lceil+$ and negative $\lceil-$ returns are represented separately. The same parameters as for the super bull regime have been used (learning interval is fixed to 15 days and the prediction horizon is fixed to 5 days). The same quantities as in figure 7,8 are represented. For information on how the figures are constructed, see the main text.

FIG. 15.

FIG. 16. Super-bear \rceil : comparative statistical tests of the predictions of our theory (average approximant S^*) represented by crosses, a trend following strategy (linear approximation of S_1) represented by open squares and the bare parabolic parameterization (3) represented by open circles, for the twelve assets presented in figure 1-6. For information on how the figures are constructed, see the main text.

FIG. 17. “Phase diagram” of the balanced-bear regime \rceil , defined in the parameter space $(\Delta T/T_N, |F|)$ with $T_N = 1$, delineating the regions of positive and negative returns. The boundaries $F_1(\Delta T)$, $F_2(\Delta T)$ and $F_3(\Delta T)$ are shown as dashed, continuous and dotted lines respectively. The dotted-dashed line indicated as “regression” on the figure corresponds to the solution of $S_0(T_N + \Delta T, F) - S_0(T_N, F) = 0$.

FIG. 18. Predicted return R of the balanced-bear regime \lfloor , defined by equation (14), as a function of the ratio $\Delta T/T_N$ of the prediction horizon over the learning interval for several values of the Froude number.

FIG. 19.

FIG. 20.

FIG. 21.

FIG. 22. Balanced bear case \lfloor : Comparative statistical tests of the predictions of our theory (average approximant S^*) represented by crosses, a trend following strategy (linear approximation of S_1) represented by open squares and the bare parabolic parameterization (3) represented by open circles, for the twelve assets presented in figure 1-6. The predictions of positive $\lfloor+$ (p7) and negative $\lfloor-$ (p8) returns are represented separately. The same parameters as for the super bull regime have been used (learning interval is fixed to 15 days and the prediction horizon is fixed to 5 days). The same quantities as in figure 7,8 are represented. For information on how the figures are constructed, see the main text.

This figure "fig1.jpg" is available in "jpg" format from:

<http://arXiv.org/ps/cond-mat/9910047v1>

This figure "fig2.jpg" is available in "jpg" format from:

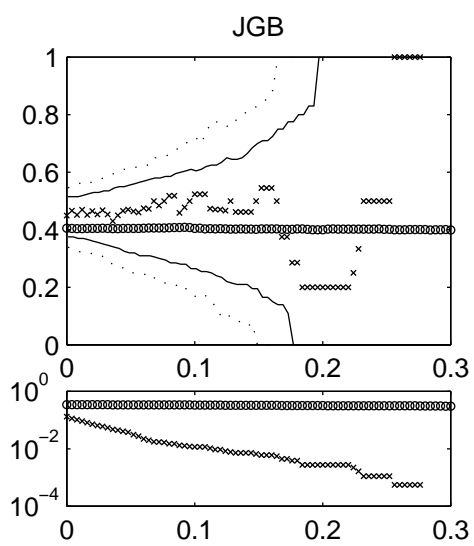
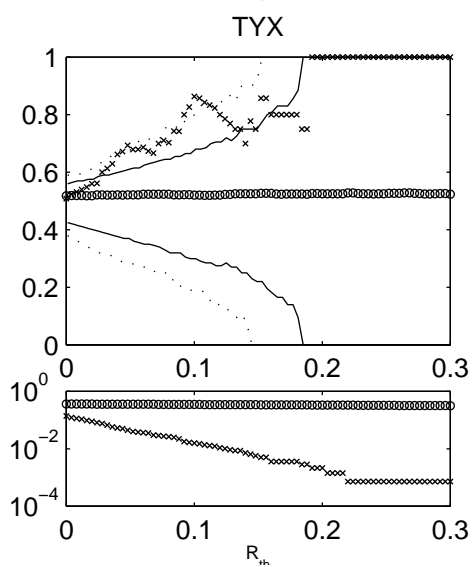
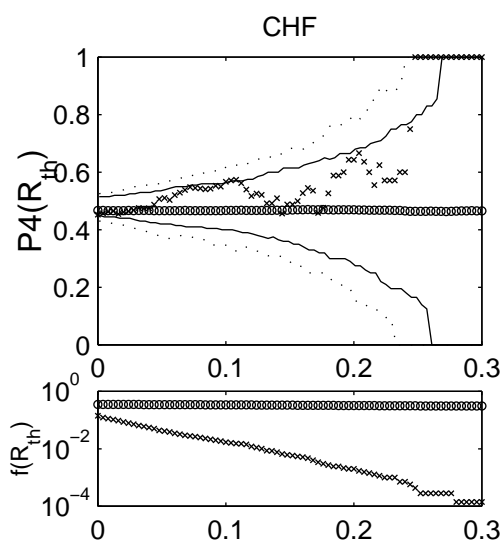
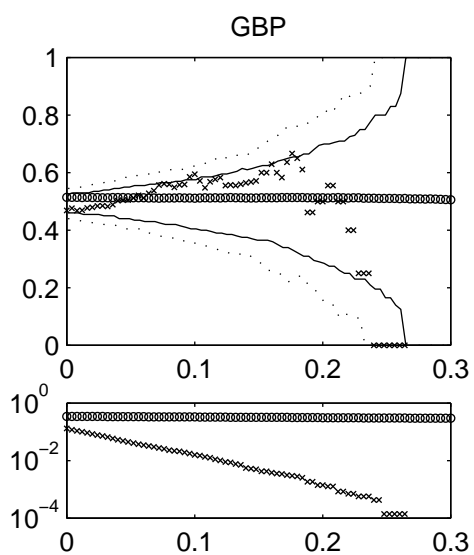
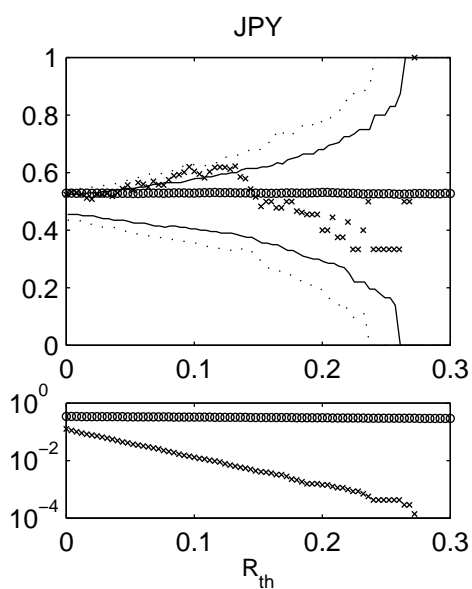
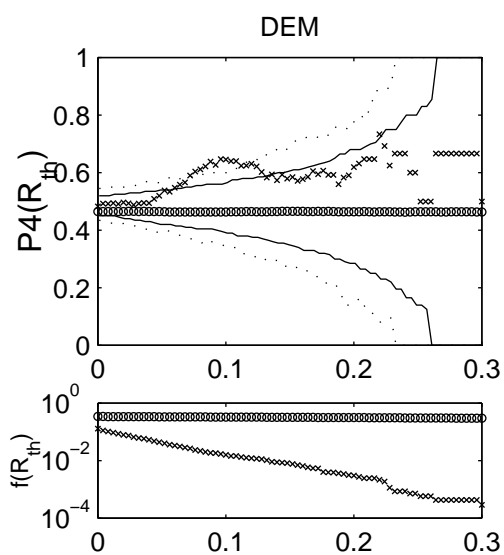
<http://arXiv.org/ps/cond-mat/9910047v1>

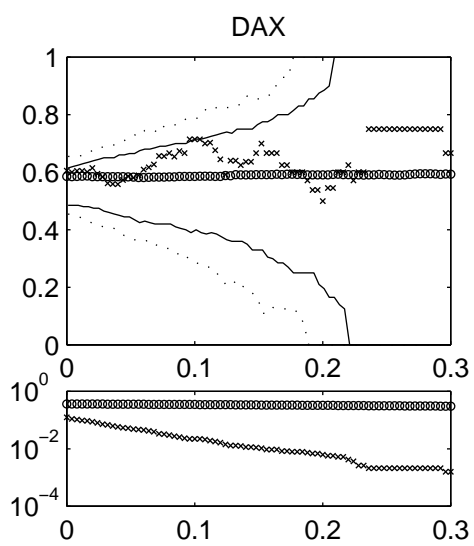
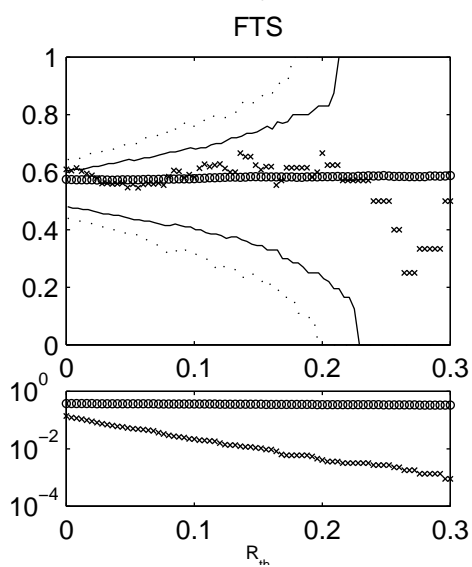
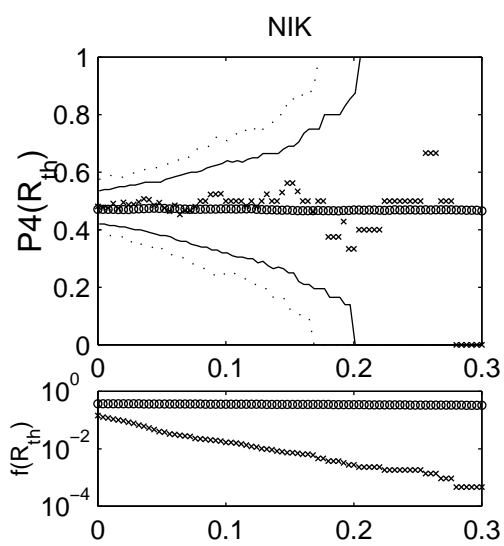
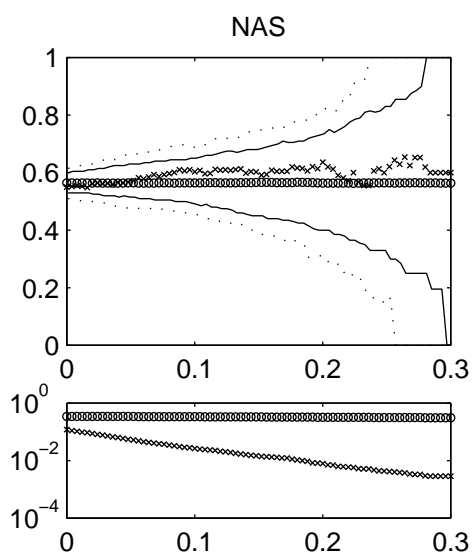
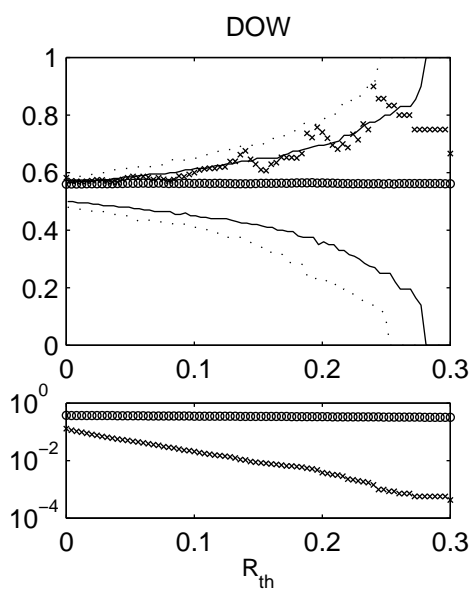
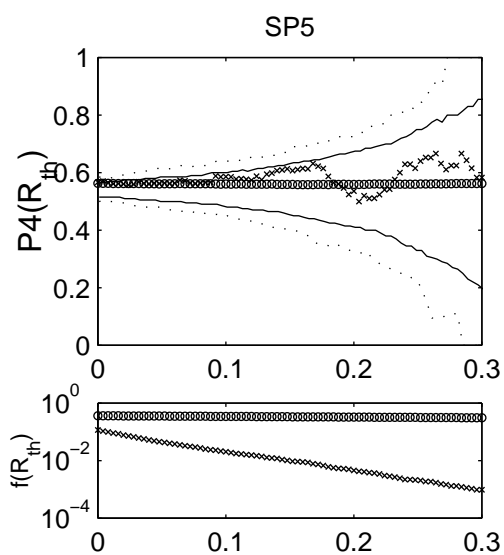
This figure "fig3.jpg" is available in "jpg" format from:

<http://arXiv.org/ps/cond-mat/9910047v1>

This figure "fig4.jpg" is available in "jpg" format from:

<http://arXiv.org/ps/cond-mat/9910047v1>





This figure "fig5.jpg" is available in "jpg" format from:

<http://arXiv.org/ps/cond-mat/9910047v1>

This figure "fig6.jpg" is available in "jpg" format from:

<http://arXiv.org/ps/cond-mat/9910047v1>

This figure "figBalBear.jpg" is available in "jpg" format from:

<http://arXiv.org/ps/cond-mat/9910047v1>

This figure "figBalBearret.jpg" is available in "jpg" format from:

<http://arXiv.org/ps/cond-mat/9910047v1>

This figure "figBalBullret.jpg" is available in "jpg" format from:

<http://arXiv.org/ps/cond-mat/9910047v1>

This figure "figBalbull.jpg" is available in "jpg" format from:

<http://arXiv.org/ps/cond-mat/9910047v1>

